

Phenomenology of High-Current Discharge in N₂ and He at Medium Pressures between Two Electrodes of Rail Geometry

Yu. S. Akishev^{a,*}, T. Alekseeva^a, V. Karalnik^a, and A. Petryakov^a

^a Troitsk Institute of Innovative and Thermonuclear Research, Moscow, Troitsk, 108840 Russia

*e-mail: akishev@triniti.ru

Received November 3, 2022; revised December 19, 2022; accepted December 26, 2022

Abstract—Plasma accelerators that form high-speed plasma jets due to the force action of their own magnetic field operate at high currents. Because of that, current spots with a high current density may occur on their electrodes, which lead to erosion of the electrodes and limit their life-time. In this work, the current modes of a plasma accelerator were investigated both without current spots and with current spots on the electrodes. In the latter case, the dynamics of current spots in the course of plasma acceleration was explored. This issue was studied by the example of a high-current ($I \leq 25$ kA) pulse discharge created between two long ($l = 30$ cm) and parallel stainless-steel electrodes of cylindrical shape of 10 mm in a diameter. Two distances between the cylinders' axes, $h = 30$ and 22 mm, were used. Two discharge zone configurations were investigated. In one of them, the discharge zone is not confined by side dielectric walls. In other one, the discharge zone is confined with transparent dielectric walls spaced by 12 mm. The high-current discharge was studied in nitrogen and helium at moderate pressures from $P = 4$ to 50 Torr. The high current was provided due to the discharging of a capacitor battery $C = 1000$ μ F charged up to the voltage $U \leq 5$ kV. At the very beginning, the discharge was initiated locally at one end of the electrodes, and then the formed plasma quickly moves toward the opposite end under strong force influence of its own magnetic field. Eventually, plasma clot is flying out of the discharge zone.

Keywords: high-current discharge rail geometry in nitrogen and helium, plasma clot motion, high-speed plasma jets

DOI: 10.1134/S1063780X2260181X

1. INTRODUCTION

Plasma accelerators that form hot and high-speed (up to 100 km/s) plasma jets due to the force action on the plasma by its own magnetic field are of great interest to science and practice [1, 2]. For example, these accelerators can be used as an effective tool for plasma modification of various surfaces, in particular, for the surface hardening of metallic products operating under extreme conditions. The plasma jet velocity at the accelerator exit depends on the total electric current passing through the accelerator, that is, the higher current, the higher velocity. Therefore, high-speed plasma accelerators have to operate at high currents. In this case, the current spots with a high current density may occur on the electrodes, sometimes called the micro-arcs or the cathode and the anode spots, which can lead to erosion of the electrodes and limit their life-time.

Despite the fact that the existence of “micro-arcs” on the electrodes of plasma accelerators have been established for a long time, the mechanisms of their occurrence and functioning remain unclear until now. The possible reasons that make it difficult to establish these mechanisms are the high current density, suffi-

ciently large size, fast time of their occurrence and short lifetime compared to the known micro-arcs or to the cathode and the anode spots on the electrodes of real arc discharges. For example, non-stationary arc cathode spots described in many papers [3–8], have a current density of no more than 3×10^4 A/cm², a diameter of no more than 100 microns, a speed of movement on the cathode surface no more than 3 m/s and a lifetime of no more than several hundred microseconds. The all listed parameters are far from those for “micro-arcs” on the electrodes of plasma accelerators. In addition, there is a problem to perform visual observation of the current spots' behavior in real plasma accelerators, since they, as a rule, have a coaxial configuration with an opaque external electrode. This problem is absent in the accelerator with rail electrodes placed between transparent side walls.

This article presents the results of experiments to study the dynamics of high-current discharge in nitrogen and helium at medium pressures in a plasma accelerator with rail geometry of electrodes. Visually, the discharge zone exhibits itself in the form of a brightly glowing plasma clot moving rapidly along the electrodes through the background gas. The images of

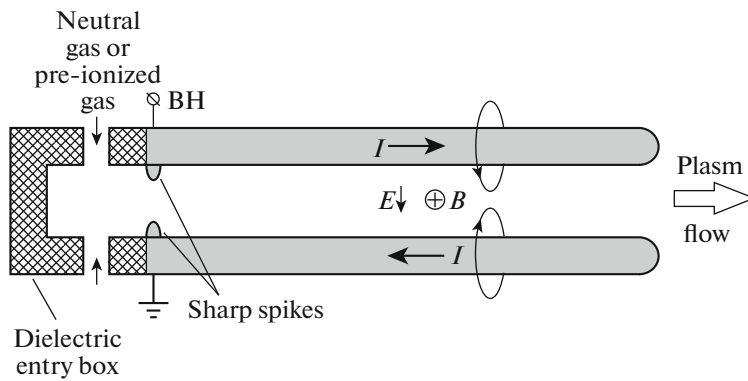


Fig. 1. The sketch of the plasma accelerator with a rail geometry of electrodes. The information on the way how to prepare the pre-ionized gas is given in the text below.

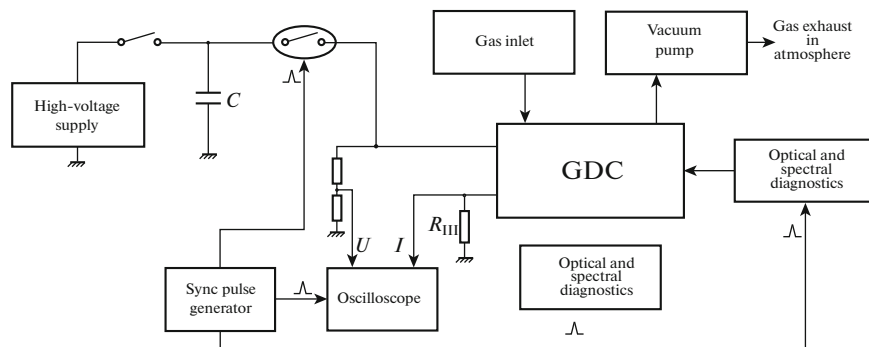


Fig. 2. The functional scheme of the experimental setup. The GDC is the gas discharge chamber.

both a moving plasma clot and near-electrode spots were captured by a fast ICCD camera synchronized with an applied voltage. A set of results on the spatio-temporal dynamics of a moving plasma clot, as well as data on the structure and dynamics of the anode and the cathode current spots coupling the current between the electrodes and the plasma in the bulk is presented. Some speculations on the cathode spots are given.

2. EXPERIMENTAL

The sketch of the plasma accelerator with rail geometry of electrodes is shown in Figure 1 that is pictured not in a real scale. Tightly to the input part of the accelerator, the dielectric entry box is located. The neutral gas or pre-ionized gas is injected in this box.

The full functional scheme of the experimental installation is shown in Fig. 2, where the GDC is a gas discharge chamber with the electrodes of rail geometry mounted inside. Synchronous operation of all elements of the installation is provided by a sync pulse generator. High-current ($I \leq 25$ kA) pulse discharge was created in the gap between two long ($l = 30$ cm)

and in parallel stainless-steel electrodes of cylindrical shape of 10 mm in a diameter. Two distances between the cylinders' axes, $h = 30$ and 22 mm, were used. Conditionally, these distances further called long and short ones. Two discharge zone configurations were investigated. In one of them, the discharge zone is not confined by side dielectric walls. In other one, the discharge zone is confined with transparent plane dielectric walls spaced by 12 mm. The high current was provided due to the discharging of a capacitor battery $C = 1000$ μ F charged up to the voltage $U \leq 5$ kV. The high-current discharge was generated in nitrogen and helium at low and moderate pressures ($P_{N_2} = 4$ and 50 Torr, and $P_{He} = 35$ and 50 Torr).

The accelerator operates as follows. At the very beginning, the discharge was ignited locally at one end of the electrodes called the enter part of plasma accelerator. After that, the formed plasma quickly moves toward the opposite end under the Ampere force created by its own strong magnetic field. Eventually, plasma clot is flying out of the discharge zone. To provide fast and controlled formation of the high discharge current, two approaches were used for creation of seed plasma at the enter part of plasma accelerator.

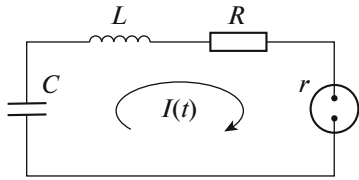


Fig. 3. Equivalent electric scheme of the studied high-current gas discharge system. $C = 1000 \mu\text{F}$, $R = 0.21 \text{ Ohm}$, $L = 2.5 \mu\text{H}$, $r \approx 0.02\text{--}0.03 \text{ Ohm}$ is the plasma resistance.

First of them is based on the usage of two short metallic spikes oriented towards each other and located on the cathode and the anode. The sharp spikes enhance strongly the local electric field strength that promotes the fast breakdown. This approach was applied to the electrode system with long inter-electrode gap ($h = 30 \text{ mm}$). The second approach is based on injection of seed plasma into the enter part by the plasma jets generated by two groups of coaxial dielectric barrier discharges. Each group consists of 9 dielectric tubes of 2.5 mm in a diameter evenly spaced within a square of $12 \times 12 \text{ mm}^2$. The plasma jets of each group are exactly oriented towards each other. This approach was applied to the electrode system with short inter-electrode gap ($h = 22 \text{ mm}$).

In the case of a high-current system, it is necessary to take into account the inductance of the external circuit. Equivalent electric scheme of the studied high-current gas discharge system is shown in Fig. 3.

The letter L denotes the distributed inductance of the external circuit which is difficult to measure in advance. Therefore, the magnitude L was found as a result of fitting the calculated discharge voltage $U_{\text{calc}}(t)$ to the experimentally measured discharge voltage $U_{\text{exp}}(t)$. This calculation was done with the use of the Kirchhoff equation when the experimentally measured current $I_{\text{exp}}(t)$ was substituted into this equation. When calculating, the battery charging voltage U_0 is assumed to be preset.

$$U_{\text{calc}}(t) = U_0 - I_{\text{exp}}(t)R - \frac{1}{C} \int_0^t I_{\text{exp}}(t) dt - \frac{dI_{\text{exp}}}{dt} L$$

under our experimental conditions, the external circuit resistance R is approximately 10 times higher than the high-current discharge resistance r . In this case, the discharge current was not determined by the discharge itself, but was set by an external circuit. In other words, the experiments were performed in the mode of a given current $I(t) \approx U_c(t)/R$, where $U_c(t)$ is the voltage on the capacitor bank.

3. RESULTS

To begin with, Fig. 4 shows the time behavior of the electrical parameters of high-current discharge in

nitrogen at low ($P = 4 \text{ Torr}$) and moderate pressure ($P = 50 \text{ Torr}$) with a large interelectrode gap ($h = 30 \text{ mm}$) under applying the voltage of the capacitor battery charged up to $U_0 = 5 \text{ kV}$. The high-current discharge in helium at $P = 35$ and 50 Torr with a short interelectrode gap ($h = 22 \text{ mm}$) under applying the voltage of the capacitor battery charged up to $U_0 = 5 \text{ kV}$ exhibits a similar behavior.

Note that the time interval in Figs. 4a, 4c is shorter compared to that in Figs. 4b, 4d despite the time behavior of the discharge current does not depend on the plasma parameters and is determined by the ballast resistor of the external circuit. The choice of the time interval on the graphs was determined by the time of flight of the plasma clot along the entire length of the electrodes. This time depends on the velocity of the plasma clot—at a lower gas pressure, the velocity is greater.

One can see in Fig. 4 that for all pressures of N_2 the maximal discharge power is about of 20 MW and total energy deposition in the plasma is huge and exceeds of 1 kJ . It means with a high probability that the plasma blowing out the accelerator contains practically fully dissociated nitrogen and is close to be almost fully ionized plasma. In other words, such accelerator can be used not only for creation of the high velocity plasma jet but for generation of plasma with extremely high parameters as well.

Figure 5 shows the image of high-current discharge in nitrogen ($P = 50 \text{ Torr}$, $U_0 = 5 \text{ kV}$) with a large interelectrode gap ($h = 30 \text{ mm}$). It looks like more or less homogeneous discharge occupying the entire length of the rail electrodes. In fact, as we will see further, the discharge represents itself as a plasma clot of finite size that fast moves along the electrodes. The picture in Fig. 4 was taken by the camera at a long exposure time exceeding the time spent by plasma clot on passage entire length of the electrodes. Thus, this picture is the superposition of instant images of the fast-moving plasma clot. One can see in Fig. 5 that there are many electrode spots and current filaments originated from these spots. The fact that these spots and filaments in fast-moving plasma clot are observed in picture taken at long exposure time indicates that they are short living but quickly appearing again in new places as the clot moves. Note the brightness of the discharge glow is very high in the first third of the electrode system (left side in the photo), therefore, to attenuate the light entering the camera, this part of the discharge zone was screened with a filter.

In this mode, as one may see (Fig. 5a), there are the current spots on the rail electrodes. Visually, the discharge in N_2 at $P = 50 \text{ Torr}$ consists of diffuse and constricted regions. The latter have the form of current filaments tilted in the direction of gas discharge movement and resting on the near-electrode current spots. The transverse size of the discharge is approximately equal to the interelectrode distance (Fig. 5b). In the

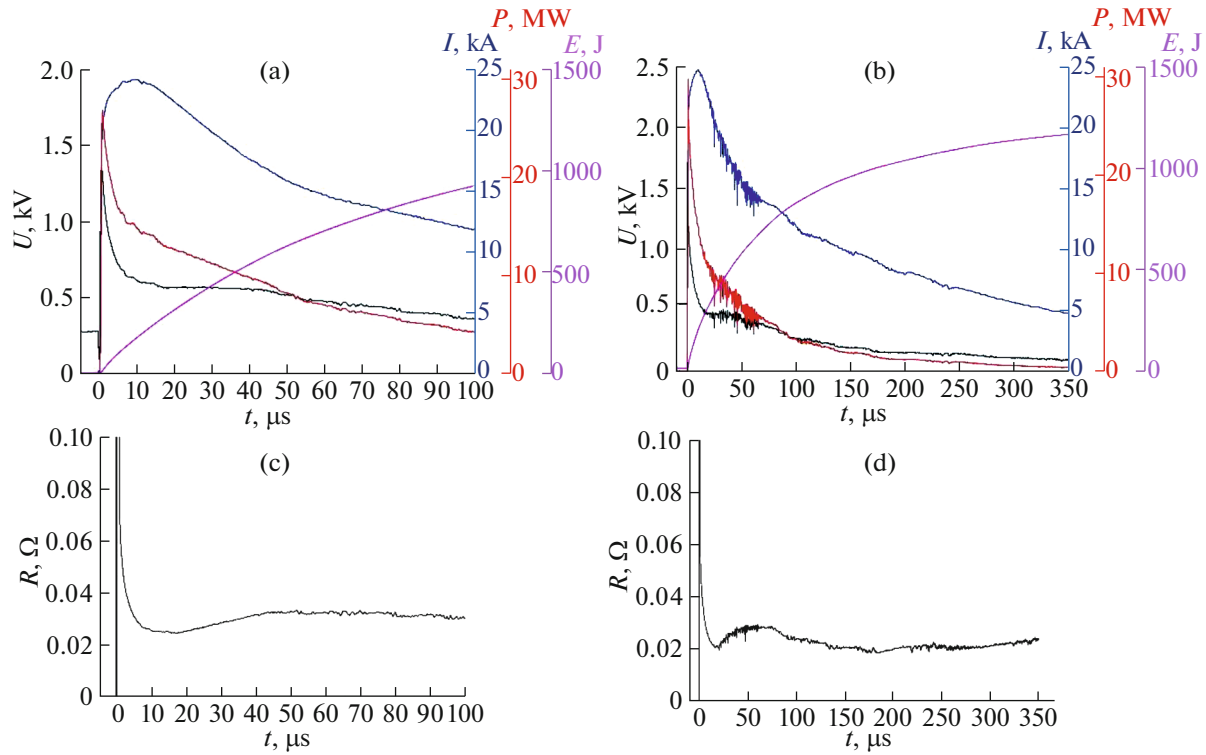


Fig. 4. The change in time of the high-current discharge electrical parameters (voltage U , current I , power W , energy deposition E). (a) $P_{N_2} = 4$ Torr; (b) $P_{N_2} = 50$ Torr; (c) plasma resistance, $P_{N_2} = 4$ Torr; (d) plasma resistance, $P_{N_2} = 50$ Torr. Everywhere, $U_0 = 5$ kV.



Fig. 5. The image of high-current discharge obtained by camera under long exposure time. (a) Side view; (b) front view. The cathode is bottom electrode. Nitrogen, $P = 50$ Torr, $h = 30$ mm, $U_0 = 5$ kV, $I_{\max} = 25$ kA.

case of N_2 at low pressure ($P = 4$ Torr), the discharge is homogeneous, that is, the current filaments and the cathode and the anode current spots on electrodes are absent. The same situation was also observed in the case of helium in short gap ($h = 22$ mm) at $P = 35$ and 50 Torr.

The force pushing the plasma clot in the accelerator is determined by the gradient of magnetic field. Therefore, it is of great interest to make estimations of the magnetic induction, B , and magnetic pressure, P_B , created in the discharge between rod electrodes of rail geometry. We assume that the azimuthal component of the local magnetic induction $B_\phi(x, t)$ from one rod is determined by the local value of the current $I(x, t)$ flowing along the rod (x is the coordinate along the

axis symmetry of rail electrodes, $x = 0$ corresponds to the accelerator enter):

$$B_\phi(x, t)[T] = \mu_0 I(x, t) / 2\pi\rho,$$

where $\mu_0 = 4\pi \times 10^{-7}$ H/m is the magnetic permeability of the vacuum, ρ is the current radius (in m) measured from the axis of the rod. The total magnetic induction is sum of the inductions of two rods:

$$B_\phi(x, t) = \frac{\mu_0 I(x, t)}{2\pi} \left[\frac{1}{\rho} + \frac{1}{h - \rho} \right].$$

The volume density of the magnetic energy or magnetic pressure, P_B , is described as follows:

$$P_B = B_\phi^2 / 2\mu_0 \text{ [J/m}^3\text{]} \quad \text{or} \quad P_B \text{ [atm]} \approx \left(\frac{B[\text{T}]}{0.501} \right)^2.$$

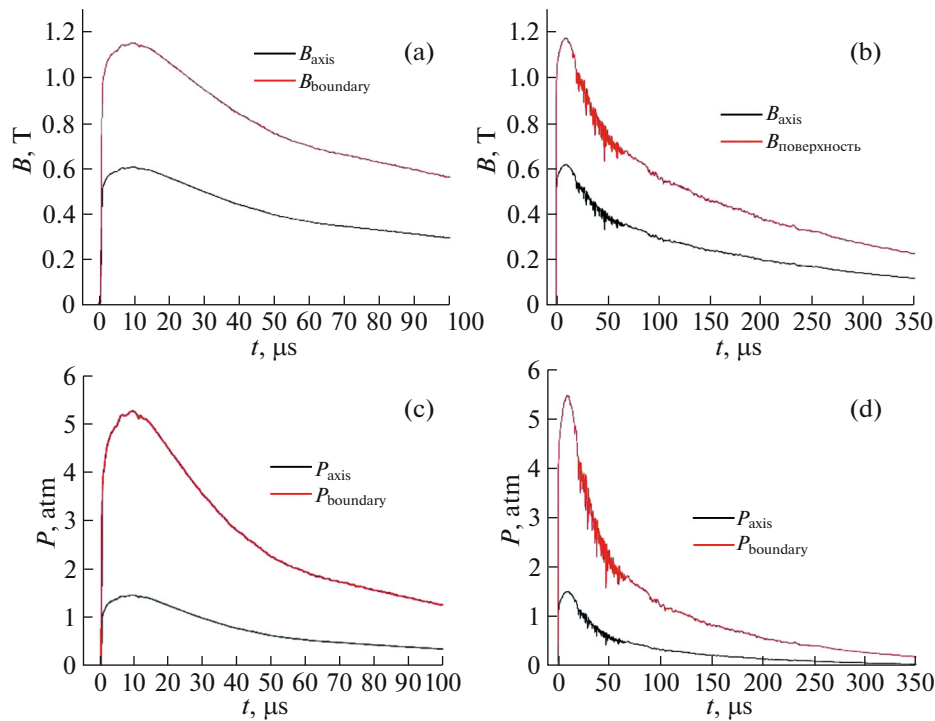


Fig. 6. Time behavior of the local magnetic induction, $B(t, x = 0)$, and magnetic pressure, $P_B(t, x = 0)$, at the rods' side surfaces and the rail geometry axis. $B_{axis}(t)$ and $B_{surface}(t)$: (a) $P_{N_2} = 4$ Torr; (b) $P_{N_2} = 50$ Torr. $P_{axis}(t)$ and $P_{surface}(t)$: (c) $P_{N_2} = 4$ Torr; (d) $P_{N_2} = 50$ Torr. Everywhere, $h = 30$ mm, $U_0 = 5$ kV.

Maximum and minimum of the magnetic pressure locate at the rods' side surfaces (on their surface) and around the axis symmetry of the rail electrodes, that is, at the radii $\rho = d/2$ and $\rho = h - d/2$ and $\rho = h/2$, respectively, where d is the rod diameter; the radius ρ is reckoned from the axis of the lower rod. Figure 6 gives the quantitative information on the time behavior of the local magnetic induction, $B(t, x = 0)$, and magnetic pressure, $P_B(t, x = 0)$, at the rods' side surfaces and the rail geometry axis for the case of nitrogen at pressures $P = 4$ and 50 Torr.

Due to that the accelerator operates in the regime with the current $I(t)$ determined by the external circuit, the magnitudes of the $B_{axis}(t)$ and $B_{surface}(t)$, the $P_{axis}(t)$ and $P_{surface}(t)$ practically do not depend on gas pressure and even on sort of gas. However, the P_B/P_{gas} ratio depends significantly on gas pressure. For instance, maximal magnitudes of the P_B/P_{gas} ratio at the rods' side surfaces are equal approximately to 1000 and 83 for $P_{N_2} = 4$ and 50 Torr, respectively. The similar situation happens in accelerator with helium as working gas. This circumstance significantly affects both the plasma clot structure and the clot velocity when moving along the electrodes. Such information was obtained when shooting the discharge image with using an 8-frame high-speed ICCD camera with an exposure of 60 ns frames and variable interval between

frames. The obtained results are shown in the figures below.

Figure 7 represents the current and voltage oscillograms corresponding to the regimes for which the discharge images were taken. The vertical color lines point the time moments for which the shots in Figs. 8 and 9 are presented. For convenience, these lines are given in different colors and divided into two groups, marked with roman numerals I and II. These groups cover the most interesting time intervals at which the discharge current exceeds 10 kA. In order to reduce the article volume, the pictures of the remaining groups are not provided.

The similar sets of the discharge images were done for the case of helium as working gas at pressures varied from 20 to 50 Torr. The obtained results are presented in Figs. 10 and 11.

The photos like those presented in Figs. 8–11 were used to calculate the velocity of the plasma clot front versus coordinate x along the rail electrode. The obtained results for different parameters of the experiments (sort of gas and its pressure, the applied voltage, the inter-electrode gap), are presented in Fig. 12.

In general, the results related to the plasma velocity at the accelerator outlet are quite expected, that is, at the fixed magnitude of the total discharge current, the outlet velocity grows with both diminishing the gas pressure and choosing the lighter gas. These facts are

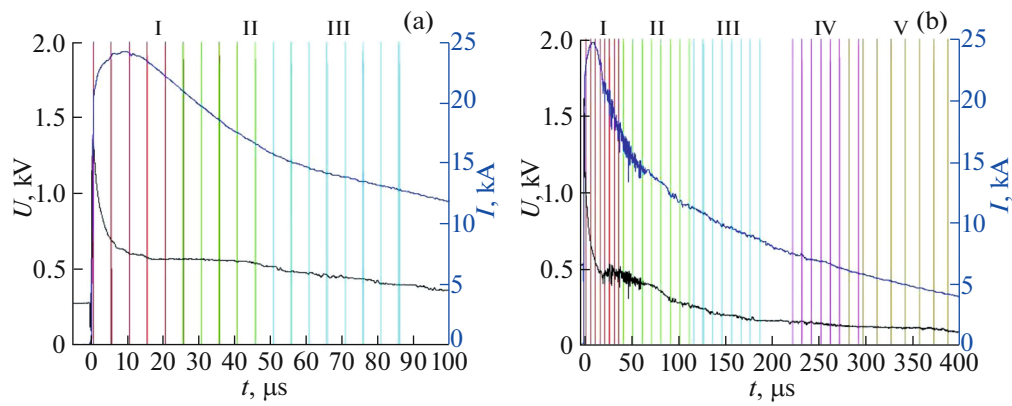


Fig. 7. The current and voltage oscillograms of the regimes for which the discharge shots in Figs. 8 and 9 were taken. The vertical color lines point the time moments which the shots are presented for. Time interval between lines is $5 \mu\text{s}$. (a) Nitrogen, $P = 4 \text{ Torr}$; (b) $P = 50 \text{ Torr}$. $H = 30 \text{ mm}$, $U_0 = 5 \text{ kV}$.

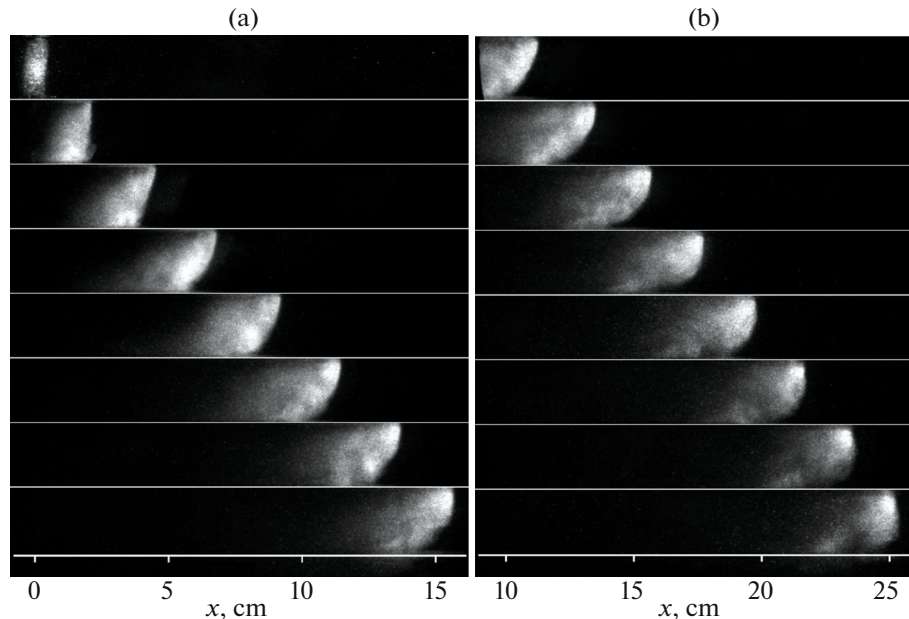


Fig. 8. Two series of the discharge images showing the shape evolution of plasma clot moving along the rails. The movement from left to right. These images correlate with the $I-U$ oscillograms in Fig. 7a. Time interval between shots is $5 \mu\text{s}$, $h = 30 \text{ mm}$. Nitrogen, $P = 4 \text{ Torr}$. $U_0 = 5 \text{ kV}$.

in agreement with other works [9–11]. However, the revealed plasma clot velocity distribution along the electrodes is new experimental information. The obtained distribution points the necessity on the correct choosing of the electrodes length to get the maximum velocity at the accelerator outlet. This statement is related to any working gas but not only to nitrogen and helium.

The experiment showed that after the plasma clot ejection from the accelerator, the unwanted arc discharge is formed between the ends of the rail electrodes. This discharge continues till the full discharg-

ing the capacitor battery. The arc discharge image is sketched in Fig. 13a. A current spot with a high current density is formed on a high-voltage electrode (anode). At the cathode, the discharge is diffuse. The consequences for the end parts of rail electrodes after many accelerator launches are shown in Fig. 13b. As can be seen, the anode is destroyed most of all due to its melting at the point of the anode spot binding. Bending the ends of electrodes in opposite directions practically eliminated the formation of a parasitic arc discharge at the output end of the accelerator.

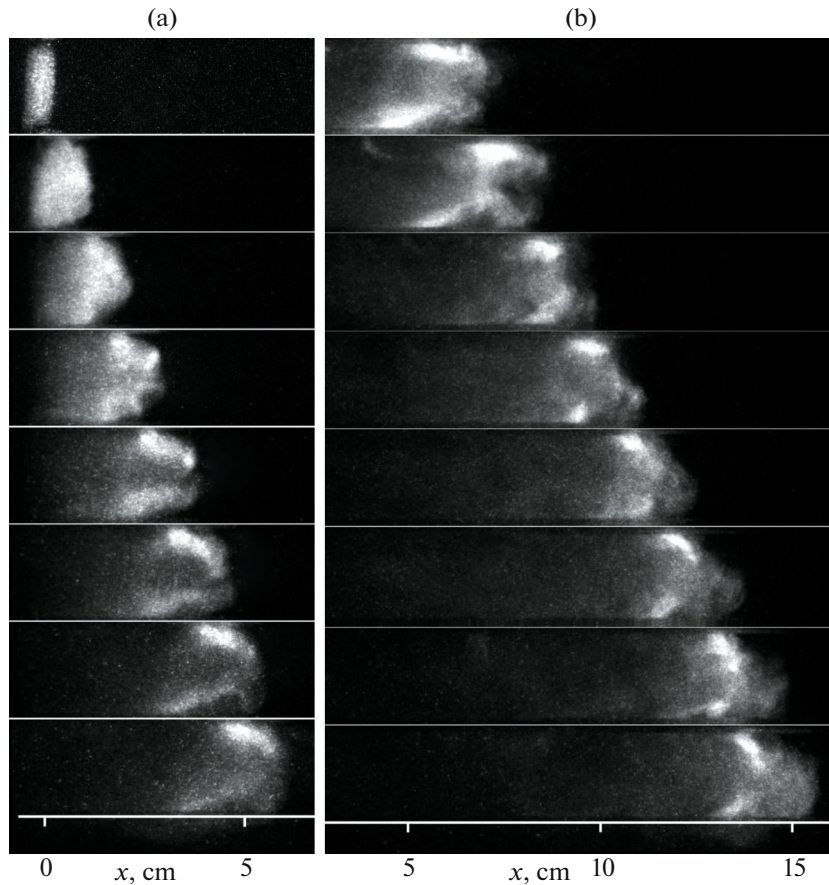


Fig. 9. Two series of the discharge images showing the shape evolution of plasma clot moving along the rails. The clot movement from left to right. These images correlate with the $I-U$ oscillograms in Fig. 7b. Time interval between shots is $5 \mu\text{s}$ for (a) (series I in Fig. 7b) and $10 \mu\text{s}$ for (a) (series II in Fig. 7b). Nitrogen, $P = 50 \text{ Torr}$, $h = 30 \text{ mm}$, $U_0 = 5 \text{ kV}$.

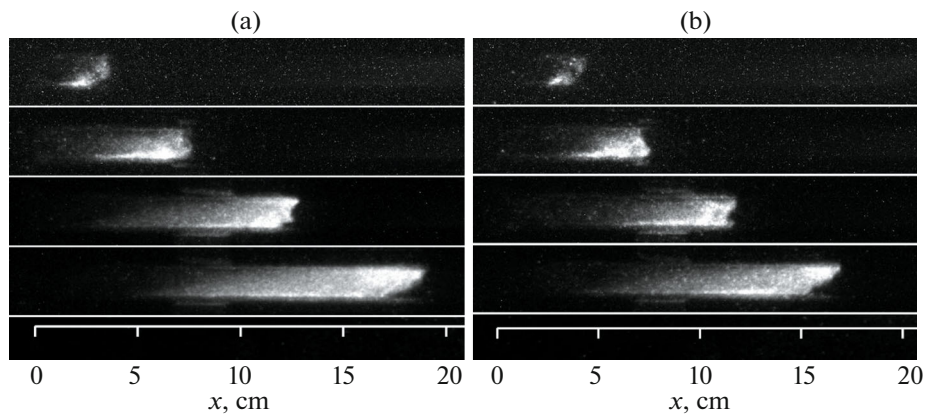


Fig. 10. The set of discharge images showing the shape evolution of plasma clot moving along the rails. Helium, $P = 20 \text{ Torr}$, $h = 22 \text{ mm}$. (a) $U_0 = 4 \text{ kV}$; (b) $U_0 = 5 \text{ kV}$. In both cases, time interval between shots is $5 \mu\text{s}$.

The images of the working surface of the anode (1) and cathode (2) after a series of discharge starts are shown in Fig. 14. As can be seen, the anode practically does not change the state of the surface except for its

terminal part (Fig. 13b), which is strongly fused by the anode current spot. The surface condition of the working part of the cathode is identical to its terminal part (Fig. 13b).

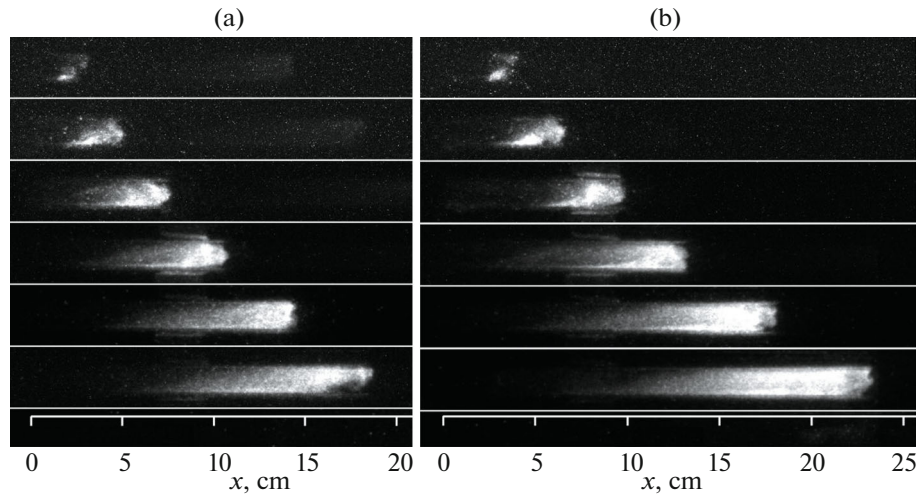


Fig. 11. The set of discharge images showing the shape evolution of plasma clot moving along the rails. (a) Time interval between shots is $2 \mu\text{s}$. Helium, $h = 30 \text{ mm}$, $P = 35 \text{ Torr}$, $U_0 = 5 \text{ kV}$. (b) Time interval between shots is $3 \mu\text{s}$. Helium, $h = 30 \text{ mm}$, $P = 50 \text{ Torr}$, $U_0 = 4 \text{ kV}$.

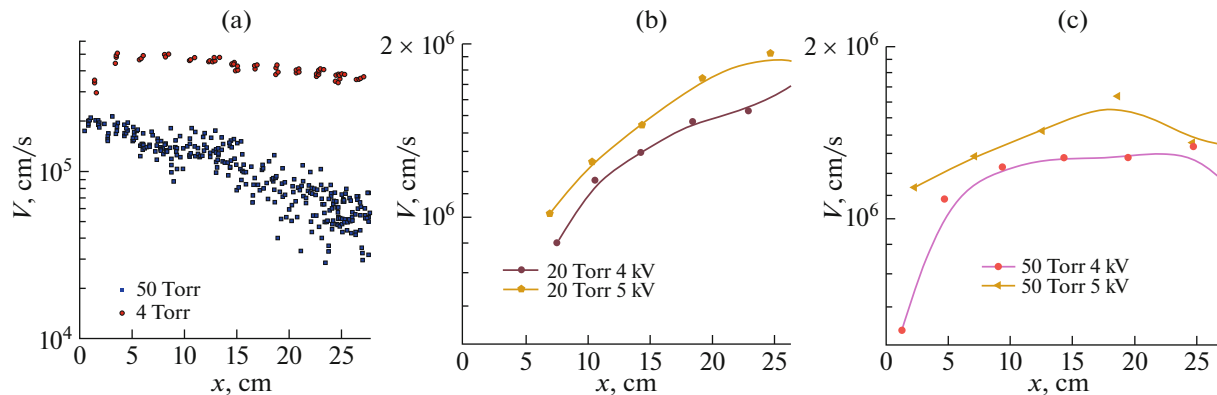


Fig. 12. The plasma clot front velocity vs. coordinate x along the electrodes for two working gases. (a) Nitrogen, $h = 30 \text{ mm}$, $U_0 = 5 \text{ kV}$; (b) helium, $h = 22 \text{ mm}$, $P = 20 \text{ Torr}$; (c) helium, $h = 22 \text{ mm}$, $P = 50 \text{ Torr}$.

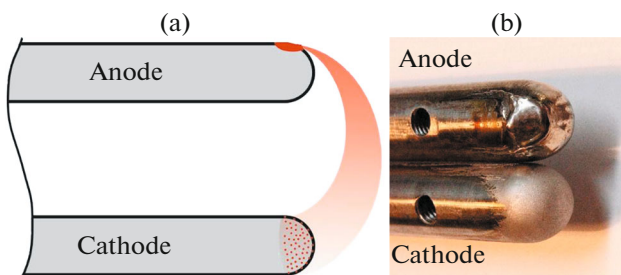


Fig. 13. The sketch of the arc discharge that is formed between the ends of the rail electrodes (a). The surface state of the end parts of rail electrodes after many launches of plasma accelerator (b).

4. DISCUSSION

The unsteady small current spots and current filaments originating from the spots were revealed on the working surface of the electrodes. According to estimation, the current density in the small spots does not exceed of 10^6 A/cm^2 . The current spots occur only in nitrogen at low plasma velocities ($V < 5.0 \text{ km/s}$) and higher pressure ($P > 50 \text{ Torr}$). In this case, the anode spots move along the electrodes continuously, while the cathode spots move by jumps. Besides, the current spots influence the clot movement. It turned out that the clot leading front, initially approximately flat and perpendicular to the direction of movement, tilts more



Fig. 14. The images of the working surface of the anode (1) and cathode (2) after a series of discharge starts. The arrow shows the place of a high-current discharge initiation. The sharp spikes initiating the discharge at this place are removed. The direction of the accelerated plasma movement is from left to right.

and more towards the cathode as the speed of the clot increases.

Small current spots are absent at low pressures ($P < 50$ Torr) in any studied gas (helium, argon, nitrogen) and at high plasma velocities ($V > 5.0$ km/s), that is, at high currents. As to absence of the anode current spots, one of the possible reasons can be related with a high plasma velocity along the electrodes. Indeed, at plasma clot velocity $V > 5.0$ km/s, the ion drift velocity is much lower than this magnitude. In such a case, for the time of the plasma clot passage along entire electrodes length, the ions starting from the anode do not come to the cathode, that is, $J_{\text{ions}} \approx 0$. It means there is no necessity in the existence of the anode layer (and the anode spot) forming the ion flow J_{ions} . Ions providing the quasi-neutrality of the plasma are formed locally in the bulk by intensive ionization processes. This is why, the current spots are absent on the anode at high plasma clot velocity.

Another situation for the cathode which has to provide the electron flow carrying the total electric current. Why are there no current spots on the cathode at a high clot velocity? Let's consider several potential mechanisms of electron emission from the cathode, which could form cathode spots.

Thermal emission of electrons. The normal operating mode of the accelerator lasts no more than 1 ms. In such a case, the massive cathode does not have time to warm up properly and remains "cold", despite the high temperature of the plasma contacting it. There-

fore, with a characteristic value of the work function $\phi \approx 4.5$ eV, the cathode temperature is not high enough to provide the necessary intensity of thermal emission of electrons.

Field-emission of electrons. The electric field on the cathode surface, even taking into account its amplification on possible irregularities of the cathode surface, does not reach the values of the order of 10^8 V/cm required for intensive electron emission.

Potential γ -emission of electrons by ions and metastables. The contribution of ions and metastables to the γ -emission of electrons is insignificant due to their rapid drift relative to the cathode by a high-speed plasma flow.

Photoemission of electrons. In principle, the emission of electrons from the cathode can be provided by intense hard VUV radiation emitted by an accelerated plasma. A list of intense VUV spectral lines that are emitted, for example, by helium plasma is presented in Table 1. As can be seen, hard photons have an energy exceeding 3–5 times the output of the cathode work function. In this case, the cathode layer may be formed at the cathode. This layer is similar to a vacuum emission diode, but with a drift transfer of electrons. The volt-ampere characteristic of such a layer does not have a negative slope. Therefore, this layer can be transversely uniform and is stable relative to the formation of the high-current spot. Thus, the photoemission of electrons by hard VUV radiation can ensure both the current transfer at the cathode and eliminate the formation of current spots on it.

In general, it can be argued that a large current in the working area of the accelerator creates an insignificant erosion effect for the electrodes. High-current arc spots forming on the output parts of the electrode system have a serious destructive effect.

CONCLUSIONS

- The electrical parameters of a high-current discharge (up to 25 kA) in nitrogen and helium at a pressure of $P = 4\text{--}50$ Torr created in the rail electrode geometry were measured.
- The presence of current spots on the cathode and anode at elevated gas pressure was revealed. The hopping character of the movement of current spots along the cathode at $P = 50$ Torr is revealed as well.
- The spatio-temporal evolution of a plasma clot during its movement under the action of an own magnetic field of a high-current discharge has been studied. The maximum magnetic pressure (5 atmospheres) was much higher than the initial pressure of the background gas.
- The absence of current spots on the electrodes was detected at low background gas pressure. The effect can be associated with a higher plasma clot velocity and maintenance of the glow cathode layer by photoemission of electrons by VUV radiation.

Table 1. Data on extremely VUV radiation of the helium atom

Wave length, nm	Energy of quant, eV
51.56168	24.0458
52.22131	23.74207
53.70299	23.08702
58.43344	21.21802

FUNDING

The work was supported by the Government contract no. N.4f.241.09.22.1127 of August 25, 2022.

CONFLICT OF INTEREST

The authors declare that they have no conflicts of interest.

REFERENCES

1. A. I. Morozov, Nucl. Fusion, Spec. Suppl., S111 (1969).
2. A. I. Morozov, *Introduction to Plasma Dynamics* (Fizmatlit, Moscow, 2006; CRC, Boca Raton, FL, 2012).
3. I. G. Kesaev, *Cathode Processes in Electric Arcs* (Nauka, Moscow, 1968) [in Russian].
4. G. A. Mesyats and Yu. D. Korolev, Sov. Phys.—Usp. **29**, 57 (1986).
5. Yu. D. Korolev and I. B. Matveev, IEEE Trans. Plasma Sci. **34**, 2507 (2006).
6. Yu. D. Korolev, O. B. Frants, N. V. Landl, V. G. Geyman, and I. B. Matveev, IEEE Trans. Plasma Sci. **35**, 1651 (2007).
7. Yu. D. Korolev, O. B. Frants, N. V. Landl, V. G. Geyman, and I. B. Matveev, IEEE Trans. Plasma Sci. **37**, 586 (2009).
8. Yu. Akishev, V. Karalnik, I. Kochetov, A. Napartovich, and N. Trushkin, Plasma Sources Sci. Technol. **23**, 054013 (2014).
<https://doi.org/10.1088/0963-0252/23/5/054013>
9. N. S. Klimov, V. L. Podkovyrov, A. M. Zhitlukhin, V. M. Safronov, D. V. Kovalenko, A. A. Moskacheva, and I. M. Poznyak, Vopr. At. Nauki Tekh., Ser.: Termoyad. Sint. **32** (2), 52 (2009).
10. D. V. Kovalenko, N. S. Klimov, A. M. Zhitlukhin, A. D. Muzychenko, V. L. Podkovyrov, V. M. Safronov, and A. D. Yaroshevskaya, Vopr. At. Nauki Tekh., Ser.: Termoyad. Sint. **37** (4), 39 (2014).
11. I. E. Garkusha, D. G. Solyakov, V. V. Chebotarev, V. A. Makhay, and N. V. Kulik, Plasma Phys. Rep. **45**, 166 (2019).